Published in final edited form as:
J Am Chem Soc. 2012 October 10; 134(40): 16488–16491. doi:10.1021/ja306854d.

Antibody-linked Spherical Nucleic Acids for Cellular Targeting

Ke Zhang[†,‡], **Liangliang Hao**[‡], **Sarah J. Hurst**, and **Chad A. Mirkin**[*]
Department of Chemistry and the International Institute for Nanotechnology, Northwestern University, 2145 Sheridan Road, Evanston, IL 60208-3113, USA

Abstract

Spherical nucleic acid (SNAs) constructs are promising new single entity gene regulation materials capable of both cellular transfection and gene knockdown, but thus far are promiscuous structures, exhibiting excellent genetic but little cellular selectivity. In this communication, we describe a strategy to impart targeting capabilities to these constructs through non-covalent functionalization with a complementary antibody-DNA conjugate. As a proof-of concept, we designed HER2-targeting SNAs and demonstrated that such structures exhibit cell type selectivity in terms of their uptake, and significantly greater gene knockdown in cells overexpressing the target antigen as compared to the analogous antibody-free and off-target materials.

Spherical nucleic acids (SNAs) are a novel class of non-viral gene regulation agents that are developing rapidly alongside conventional cationic polymer and liposomal systems.[1-7] Typically, these structures are comprised of densely functionalized and highly oriented nucleic acids covalently attached to the surface of a metallic, semiconducting, or insulating inorganic or polymeric core material.[8-11] They also can be core-less, hollow structures composed almost entirely of nucleic acid molecules.[12] Such constructs are capable of bypassing the natural defenses of biological systems for exogenous nucleic acids and inhibiting the expression of certain target genes through either antisense or siRNA pathways. [3,13,14] Consequently, SNAs offer several advantages over viral vectors and many other synthetic systems, including low toxicity, low immunogenicity, resistance to enzymatic degradation, and more persistent gene knockdown.[13-18]

Conventional approaches for transporting nucleic acids into the cytoplasm involve their complexation with cationic polymers or nanoparticles,[19-23] or the use of viral capsids.[24] These structures serve two primary purposes: they protect the nucleic acid from degradation and facilitate cellular uptake and intracellular transport.[20] The SNA, on the other hand, achieves protection and efficient delivery of nucleic acids utilizing unique properties arising from its densely packed, highly oriented nucleic acid shell.[14] We have shown that such shells create areas of high local salt concentration, which when combined with steric inhibition, serve to reduce nuclease activity and protect the nucleic acids from enzymatic degradation.[12] In addition, these SNAs recruit scavenger proteins to their surfaces from the natural extracellular environment, which facilitate endocytosis.[3,13] This pathway seems general with respect to both SNA and cell type, including primary cells.[25] However, this universal cell entry mechanism cannot distinguish diseased cells from healthy cells, thus restricting the SNA platform to uses that involve local delivery or systemic ones that result

[*]To whom correspondence should be addressed. chadnano@northwestern.edu.
[†]Current address: Department of Chemistry and Chemical Biology, Northeastern University, 360 Huntington Ave, Boston, MA 02115-5000, USA
[‡]These authors contributed equally.

Supporting Information Available: Experimental procedures, DNA sequences and additional characterization data. This materials is available free of charge via the Internet at http://pubs.acs.org.

in preferential tumor loading in the case of cancer applications. Therefore, to fully realize the potential of these constructs for systemic *in vivo* diagnostic and therapeutic applications, methods will need to be developed to target them to specific cell types of interest.[26-29]

Herein, we report the design and synthesis of a new SNA-nucleic acid-antibody conjugate that shows outstanding selectivity for cell lines with receptors recognized by the antibody. Specifically, these SNA conjugates consist of a monoclonal antibody (mAb)-DNA conjugate hybridized to an SNA containing a gold nanoparticle (AuNP) core (Figure 1A). The proof-of-concept structure has a mAb that recognizes the human epithelial growth factor receptor 2 (HER2), a member of the ErbB protein family, which is involved in signal transduction pathways leading to increased cell growth and differentiation.[30,31] By using inductively coupled plasma mass spectrometry (ICP-MS), we show that the HER2-targeting SNAs are taken up by cells expressing HER2 to a much greater extent and at a faster initial rate compared to non-targeted particles. We further demonstrate efficient antisense gene knockdown in HER2-overexpressing cell lines at remarkably low particle concentrations and using short particle exposure times. Therefore, these novel constructs point towards a way of increasing both the selectivity and potency of the SNA platform.

In a typical experiment, an azide-functionalized mAb is initially covalently conjugated with a fluorophore-labeled sense DNA sequence (sequence: 5' AGC ACC ATG GAG T_5-(fluorescein-T)-PEG_1-alkyne 3'; mAb-DNA) using the Cu(I) catalyzed Huisgen cycloaddition reaction (Click chemistry). It is important to note that the Click chemistry was performed using *in situ* generated Cu(I) as the catalyst and (trishydroxypropyltriazolylmethyl)amine (THPTA) as the ligand. THPTA is necessary to prevent the Cu(I)-induced aggregation of various proteins.[9] After reaction, residues and excess DNA were removed by fast protein liquid chromatography (FPLC). Unreacted mAb-azide was removed in subsequent centrifugation-resuspension steps (*vide infra*). When 2.0 equivalents of DNA-alkyne were reacted with 1.0 equivalent of mAb-azide, we observed the conjugation of ~1 DNA/mAb as indicated by the shift of the antibody MALDI-ToF peak from 154.2 kDa to 161.4 kDa (Figure 1B). However, the full width at half-maximum of the primary peak increased from 4 kDa to 15 kDa, indicating the actual degree of functionalization ranges from 0 to 2. Note that excess DNA-alkyne was required to maximize the number of mAbs with at least one oligonucleotide.

Once the Ab-DNA conjugates have been isolated and purified, they can be hybridized to the complementary antisense sequences that comprise the surface of a SNA AuNP conjugate[20] (5' CTC CAT GGT GCT CAC -T_{10}-SH 3', Figure 1A; antibody and DNA sequence details are in the Supporting Information, Table S1). Hybridization of the mAb-DNA to the SNA was achieved by co-incubation at 40 °C for 12 h in phosphate buffered saline containing 0.01% TWEEN 20 (PBST, pH 7.2). Thereafter, the conjugates were returned to room temperature and subjected to three sets of successive centrifugation-resuspension steps to remove unbound mAb. They were finally suspended in PBST at a particle concentration of 100 nM. To quantitatively determine the number of mAb-DNA strands associated with each SNA, we oxidatively dissolved the AuNP of the SNA (10 nM) in the presence of KCN, releasing the DNA strands from the surface. We then measured the fluorescence of these unquenched strands, and compared the results to a standard curve constructed from known fluorescent mAb-DNA concentrations. We determined that on average 1.9 mAb-DNAs were hybridized to each SNA (a mAb-DNA:SNA molar ratio of 2:1 was used during hybridization). After hybridization, the SNA hydrodynamic diameter increased from 19 to 23 nm as measured by dynamic light scattering (DLS), consistent with mAbs-DNA being tethered to the SNAs (Figure 1C).

To further verify that the mAb-DNA is hybridized to the SNAs, a melting experiment was performed in which the solution temperature was gradually increased from 20 to 80 °C while the fluorescence of the fluorophore-labeled mAb-DNA was monitored (excitation: 488 nm, emission: 515 nm). Below the duplex melting temperature (T_m, 44.9 °C), the fluorophore label on the mAb-DNA is partially quenched due to close proximity to the AuNP surface. As the temperature of the system is increased, a rise in the fluorescence is observed, indicative of dehybrization of the two strands and release of the mAb-DNA strand; when released, the fluorophore is no longer quenched (Figure S1).

To ensure that the HER2 mAb-functionalized SNAs (anti-HER2 SNAs) retain their antigen binding properties, we designed and performed a competitive binding assay to quantitatively measure the relative binding affinity of the conjugates with HER2. In this assay, mAb-conjugated structures (mAb-DNA and anti-HER2 SNA) were each mixed at room temperature with free, biotin-conjugated mAb (b-mAb) at ratios ranging from 1 to 100, and the mixtures were allowed to compete for surface-immobilized HER2. Thereafter, a streptavidin-horseradish peroxidase conjugate was used to detect the b-mAb. The binding affinity of the mAb-DNA and anti-HER2 SNA relative to b-mAb can be derived from the binding isotherms (Table S2 and Figure S2). We found that DNA conjugation to the free mAb did not significantly affect mAb recognition for HER2 ($K_{\text{free mAb}}/K_{\text{b-mAb}} = 0.37 \pm 0.05$ *vs* $K_{\text{mAb-DNA}}/K_{\text{b-mAb}} = 0.48 \pm 0.08$). When the mAb-DNA is hybridized to the SNA, its binding affinity dropped slightly, to 0.11 ± 0.02 times $K_{\text{b-mAb}}$, likely due to increased steric hindrance. In contrast, bovine serum albumin (BSA), a negative control, shows no significant binding. These data show that the anti-HER2 SNAs are excellent binders for HER2.

We next investigated if these materials preferentially bind to HER2-overexpressing cells. Results from three cell lines were compared: A549 (HER2 non-expressing), MCF-7 (moderate HER2 expression), and SKOV-3 (HER2 overexpression). Endogenous HER2 expression levels in each type of cell were confirmed by Western blotting (Figure S3). Anti-HER2 SNAs and non-mAb SNAs were incubated at 4 °C for 4 h with each set of cells. At 4 °C, cellular processes including endocytosis are inhibited and therefore the observed cell-associated particles are primarily cell surface-bound.[32] The cells were harvested and lysed for gold content analysis by using ICP-MS. When the HER2-targeted particles were used (10 nM), the SKOV-3 cells showed the highest amount of cell-associated particles of *ca.* 2.74×10^5 particles/cell (Figure 2A). This value is *ca.* 10.1 fold higher compared with the non-targeted particles. For MCF-7 cells, *ca.* 6.0×10^4 particles were found to be associated with each cell when the targeted SNAs were used, *ca.* 4 fold higher than non-targeted. In contrast, A549 cells did not show a significant difference for targeted and non-targeted particles, and all cells incubated with the non-targeting SNAs only exhibit a background level of cell-associated particles of *ca.* 5-15k particles/cell. Laser scanning confocal microscopy (LSCM) revealed that, at 4 °C, the particles were predominantly located on the exterior of the cells (Figure 3A).

While incubation at 4 °C provides information on cell-surface associated particles, it is also important to compare the cell uptake at biologically relevant temperatures (i.e., 37 °C). It is possible that non-specific, scavenger-mediated endocytosis becomes the dominant internalization mechanism, rendering the HER2-mediated endocytotic pathway insignificant. After 4 h of incubation at 37 °C, we observed an increase of cell-associated SNAs for all three cell lines using particles with or without mAb. When compared to the samples at 4 °C, the numbers were much higher (10-27 fold increase) because the energy dependent endocytosis pathway is activated. LCSM show that the SNAs are indeed primarily located within the cells (Figures 3B and S4). The anti-HER2 SNAs exhibited a slightly reduced, but nonetheless high specificity for SKOV-3 cells at 37 °C as compared to the specificity at 4 °C

(7.8 fold higher cell uptake compared with non-targeted SNAs at 10 nM *vs*. 10.1 fold for 4 °C). In MCF-7 cells, the selective advantage over non-targeted SNAs is *ca*. 2.6-5.0 fold, as the cell surface presents fewer copies of HER2 than SKOV-3 cells (Figure 2B). These data suggest that HER2-mediated endocytosis of SNAs roughly scales with non-specific, scavenger-mediated endocytosis as the temperature is increased from 4 to 37 °C. The slight drop in specificity could be due to a combined effect of cellular differences for a particular endocytosis pathway, and an inherent decrease in selectivity of the anti-HER2 mAb binding at 37 °C.[33]

We also studied the cell uptake of both targeted and non-targeted SNAs as a function of time with SKOV-3 cells. The cell selectivity diminishes as incubation time is extended beyond 24 h (Figure 4). In the first 6 h of incubation, targeted SNAs exhibit rapid cellular uptake (initial uptake rate *ca*. 236 particles·s^{-1}cell^{-1} *vs*. 19 particles·s^{-1}cell^{-1} for non-targeted). However, after 24 h of incubation, there is only a 1.2 fold increase in accumulated anti-HER2 SNA in cells relative to non-targeted SNA (Figure 4). The rate for HER2-mediated endocytosis becomes significantly reduced after 8 h, to on average 7 particles·s^{-1}cell^{-1}. The drop in rate may result from the cell's inability to rapidly replenish HER2 on its surface after mAb binding/endocytosis.[34] Nevertheless, we hypothesize that the initial cell association in the first 4 hours (6×10^6 particles/cell, Figure 2B) can lead to sufficient accumulation of the SNAs in HER2-overexpressing cells for effective gene regulation.

We performed a set of gene knockdown experiments utilizing the anti-HER2 SNAs. In this case, the DNA strands on the surface were designed to bind HER2 mRNA. Two negative controls were also included, which have either an off-target antibody (anti-His polyclonal antibody) or a scrambled antisense DNA sequence (5' GAG CTG CAC GCT GCC GTC A 3'). We incubated SKOV-3 cells with anti-HER2 SNAs and controls at 37 °C, using concentrations ranging from 50 pM to 10 nM, for 4 h. Following the incubation period, the solution was replaced with fresh growth media, and the cells were allowed to grow for another 48 h before being lysed and assayed by immunoblotting. Strikingly, we found that *using only 50 pM* of the anti-HER2 SNA, HER2 expression in SKOV-3 cells can be reduced to 12.7% of untreated cells by band density analysis, and at 1 nM, no HER2 was detected (Figure 5). In contrast, the cells treated with 1 nM of the off-target SNAs still show 48% of HER2. Particles with a scrambled sequence did not reduce HER2 expression at all concentrations tested, indicating the knockdown effect is specific.

These data show that hybridization-based tethering of the HER2 mAb to SNAs imparts cell selectivity to these particles, and allows for faster cell uptake and more efficient gene knockdown than the native SNA structures of the same sequence. Moreover, these conjugates exhibit many of the same attributes of the non-targeted SNA structures. Taken together, the targeted SNAs represent a significant step forward towards constructs that will allow for the systemic targeting of diseases with genetic bases, including many forms of cancer. Importantly, the general hybridization approach to functionalize SNAs reported herein can be extended to a wide variety of antibodies and other targeting moieties such as peptides, small molecules, and aptamers. [35-38]

Supplementary Material

Refer to Web version on PubMed Central for supplementary material.

Acknowledgments

This material is based upon work supported by the Center for Cancer Nanotechnology Excellence (CCNE) initiative of the National Institutes of Health (NIH) under Award No. U54 CA151880, the Non-equilibrium Energy Research Center (NERC), an Energy Frontier Research Center funded by the U.S. Department of Energy, Office of

Science, Office of Basic Energy Sciences under Award Number DE-SC0000989, the International Institute for Nanotechnology at Northwestern University, the Prostate Cancer Foundation, the “Dixon Translational Research Grants Initiative” of the Northwestern Memorial Foundation, Grant # R21AR062898 from the National Institute Of Arthritis And Musculoskeletal And Skin Diseases, Grant # R01AR060810 from the National Institute Of Arthritis And Musculoskeletal And Skin Diseases, and the Defense Advanced Research Projects Agency (DARPA)/ Microsystems Technology Office (MTO) under Award No. N66001-11-1-4189. The transmission electron microscopy was carried out in the EPIC facility of NUANCE Center at Northwestern University. NUANCE Center is supported by NSF-NSEC, NSF-MRSEC, Keck Foundation, the State of Illinois and Northwestern University. Mass spectrometry was conducted at the IMSERC facility at Northwestern University.

References

1. Rosi NL, Giljohann DA, Thaxton CS, Lytton-Jean AK, Han MS, Mirkin CA. Science. 2006; 312:1027. [PubMed: 16709779]
2. Cutler JI, Auyeung E, Mirkin CA. J Am Chem Soc. 2012; 134:1376. [PubMed: 22229439]
3. Giljohann DA, Seferos DS, Daniel WL, Massich MD, Patel PC, Mirkin CA. Angew Chem Int Ed. 2010; 49:3280.
4. Sandhu KK, McIntosh CM, Simard JM, Smith SW, Rotello VM. Bioconjugate Chem. 2002; 13:3.
5. Rink JS, McMahon KM, Chen X, Mirkin CA, Thaxton CS, Kaufman DB. Surgery. 2010; 148:335. [PubMed: 20633730]
6. Patel PC, Giljohann DA, Seferos DS, Mirkin CA. Proc Natl Acad Sci U S A. 2008; 105:17222. [PubMed: 19004812]
7. Dhar S, Daniel WL, Giljohann DA, Mirkin CA, Lippard SJ. J Am Chem Soc. 2009; 131:14652. [PubMed: 19778015]
8. Mirkin CA, Letsinger RL, Mucic RC, Storhoff JJ. Nature. 1996; 382:607. [PubMed: 8757129]
9. Cutler JI, Zheng D, Xu XY, Giljohann DA, Mirkin CA. Nano Lett. 2010; 10:1477. [PubMed: 20307079]
10. Li Z, Zhang Y, Fullhart P, Mirkin CA. Nano Lett. 2004; 4:1055.
11. Agbasi-Porter C, Ryman-Rasmussen J, Franzen S, Feldheim D. Bioconjugate Chem. 2006; 17:1178.
12. Cutler JI, Zhang K, Zheng D, Auyeung E, Prigodich AE, Mirkin CA. J Am Chem Soc. 2011; 133:9254. [PubMed: 21630678]
13. Giljohann DA, Seferos DS, Prigodich AE, Patel PC, Mirkin CA. J Am Chem Soc. 2009; 131:2072. [PubMed: 19170493]
14. Seferos DS, Prigodich AE, Giljohann DA, Patel PC, Mirkin CA. Nano Lett. 2009; 9:308. [PubMed: 19099465]
15. Massich MD, Giljohann DA, Seferos DS, Ludlow LE, Horvath CM, Mirkin CA. Mol Pharm. 2009; 6:1934. [PubMed: 19810673]
16. Massich MD, Giljohann DA, Schmucker AL, Patel PC, Mirkin CA. ACS Nano. 2010; 4:5641. [PubMed: 20860397]
17. Prigodich AE, Alhasan AH, Mirkin CA. J Am Chem Soc. 2010; 133:2120. [PubMed: 21268581]
18. Young KL, Scott AW, Hao L, Mirkin SE, Liu G, Mirkin CA. Nano Lett. 2012; 12:3867. [PubMed: 22725653]
19. Zhang K, Fang HF, Wang ZH, Li Z, Taylor JSA, Wooley KL. Biomaterials. 2010; 31:1805. [PubMed: 19878990]
20. Mintzer MA, Simanek EE. Chem Rev. 2008; 109:259. [PubMed: 19053809]
21. Dunn SS, Tian S, Blake S, Wang J, Galloway AL, Murphy A, Pohlhaus PD, Rolland JP, Napier ME, DeSimone JM. J Am Chem Soc. 2012; 134:7423. [PubMed: 22475061]
22. Christie RJ, Matsumoto Y, Miyata K, Nomoto T, Fukushima S, Osada K, Halnaut J, Pittella F, Kim HJ, Nishiyama N, Kataoka K. ACS Nano. 2012; 6:5174. [PubMed: 22575090]
23. Green JJ, Zugates GT, Langer R, Anderson DG. Methods Mol Biol. 2009; 480:53. [PubMed: 19085119]
24. Waehler R, Russell SJ, Curiel DT. Nat Rev Genet. 2007; 8:573. [PubMed: 17607305]

25. Patel PC, Giljohann DA, Daniel WL, Zheng D, Prigodich AE, Mirkin CA. Bioconjugate Chem. 2010; 21:2250.
26. Song E, Zhu P, Lee SK, Chowdhury D, Kussman S, Dykxhoorn DM, Feng Y, Palliser D, Weiner DB, Shankar P, Marasco WA, Lieberman J. Nat Biotechnol. 2005; 23:709. [PubMed: 15908939]
27. Kamphuis MM, Johnston AP, Such GK, Dam HH, Evans RA, Scott AM, Nice EC, Heath JK, Caruso F. J Am Chem Soc. 2010; 132:15881. [PubMed: 20977221]
28. Gao XH, Cui YY, Levenson RM, Chung LWK, Nie SM. Nat Biotechnol. 2004; 22:969. [PubMed: 15258594]
29. Lee H, Lytton-Jean AKR, Chen Y, Love KT, Park AI, Karagiannis ED, Sehgal A, Querbes W, Zurenko CS, Jayaraman M, Peng CG, Charisse K, Borodovsky A, Manoharan M, Donahoe JS, Truelove J, Nahrendorf M, Langer R, Anderson DG. Nat Nano. 2012; 7:389.
30. Hynes NE, Lane HA. Nat Rev Cancer. 2005; 5:341. [PubMed: 15864276]
31. Baselga J, Swain SM. Nat Rev Cancer. 2009; 9:463. [PubMed: 19536107]
32. Goldenthal KL, Pastan I, Willingham MC. Exp Cell Res. 1984; 152:558. [PubMed: 6144562]
33. Zeder-Lutz G, Zuber E, Witz J, Van Regenmortel MHV. Anal Biochem. 1997; 246:123. [PubMed: 9056193]
34. Hendriks BS, Opresko LK, Wiley HS, Lauffenburger D. J Biol Chem. 2003; 278:23343. [PubMed: 12686539]
35. Rasmussen UB, Schreiber V, Schultz H, Mischler F, Schughart K. Cancer Gene Ther. 2002; 9:606. [PubMed: 12082461]
36. Pan D, Turner JL, Wooley KL. Chem Commun (Camb). 2003:2400. [PubMed: 14587701]
37. Shangguan D, Li Y, Tang Z, Cao ZC, Chen HW, Mallikaratchy P, Sefah K, Yang CJ, Tan W. Proc Natl Acad Sci U S A. 2006; 103:11838. [PubMed: 16873550]
38. Galbiati A, Tabolacci C, Morozzo Della Rocca B, Mattioli P, Beninati S, Paradossi G, Desideri A. Bioconjug Chem. 2011; 22:1066. [PubMed: 21545180]

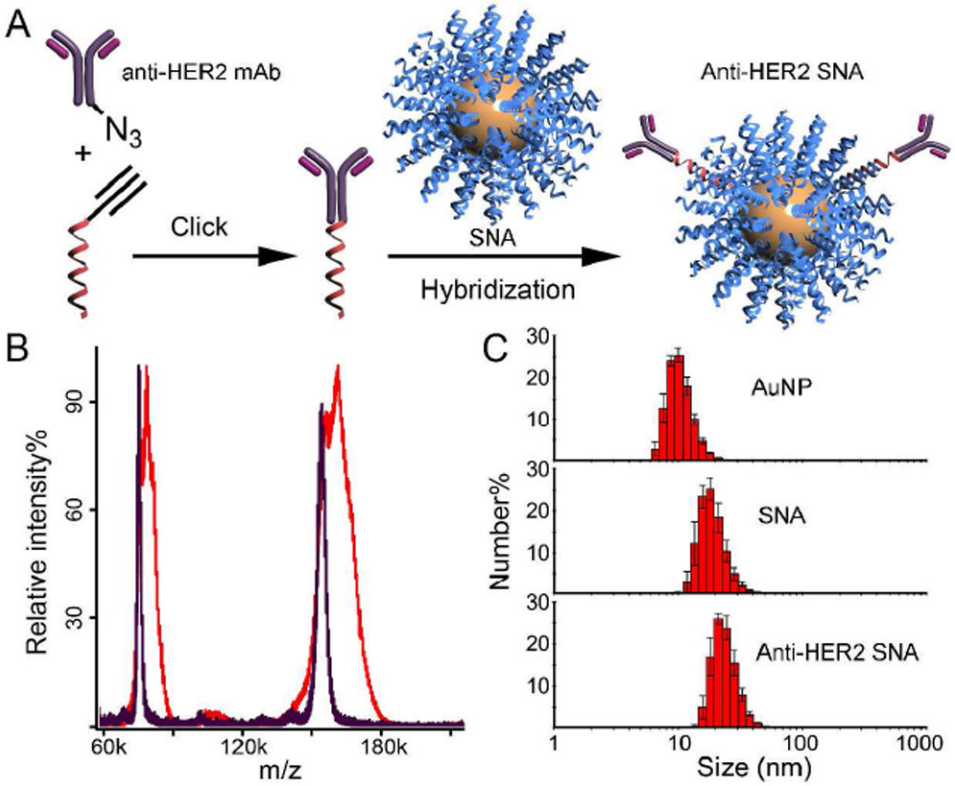

Figure 1.

(**A**) Schematic showing the synthesis of anti-HER2 SNAs. (**B**) MALDI-ToF spectra of anti-HER2 mAb (purple) and mAb-DNA conjugate (red). The m/z difference between the primary peaks is 7.2 kDa, corresponding to the mass of one sense DNA strand. (**C**) Hydrodynamic diameters of citrate stabilized AuNPs (10.4 ± 1.2 nm), SNAs (18.5 ± 2.1 nm), and anti-HER2 SNAs (23.3 ± 2.8), as measured by DLS.

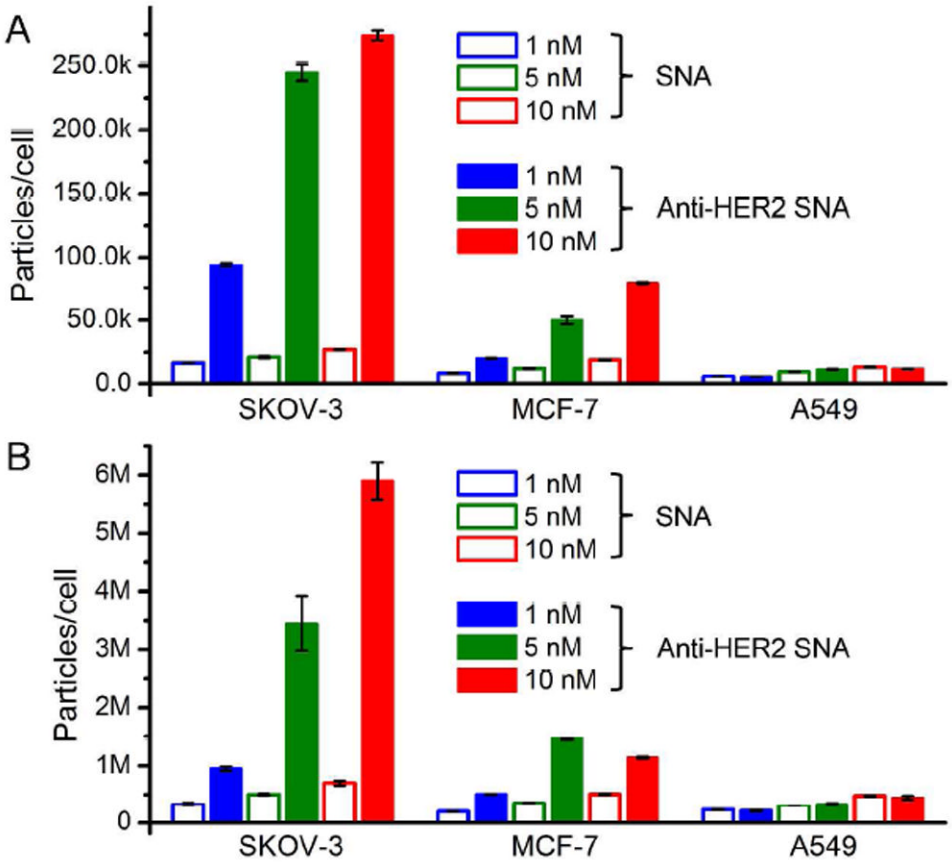

Figure 2.

Number of gold nanoparticles per cell after 4 h incubation at: (**A**) 4 °C and (**B**) 37 °C. HER2 overexpressing cells (SKOV-3) and moderate expressing cells (MCF-7) show significantly higher uptake with targeted particles, while no selectivity was found for HER2 non-expressing cells (A549).

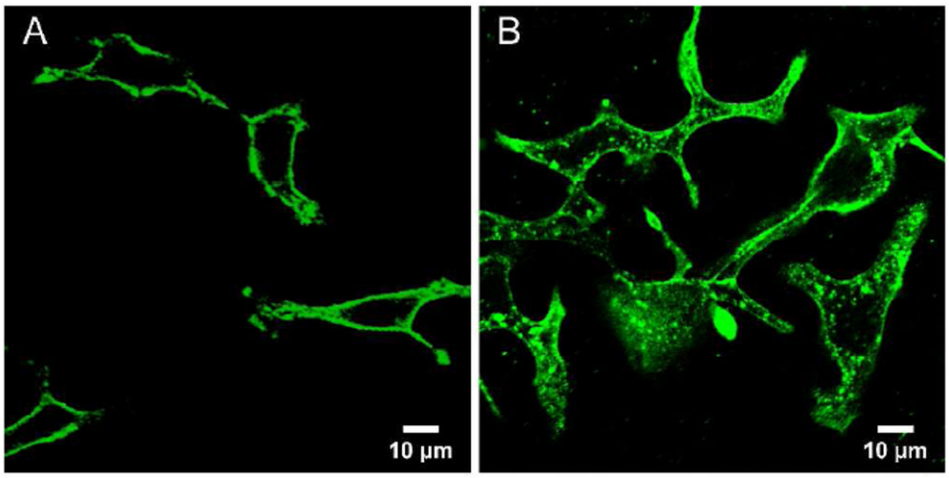

Figure 3.
Confocal micrograph of SKOV-3 cells incubated with 5 nM anti-HER2 SNAs for 4 h at: (**A**) 4 °C and (**B**) 37 °C. Anti-sense DNA strands were labeled at the 5’-end with fluorescein.

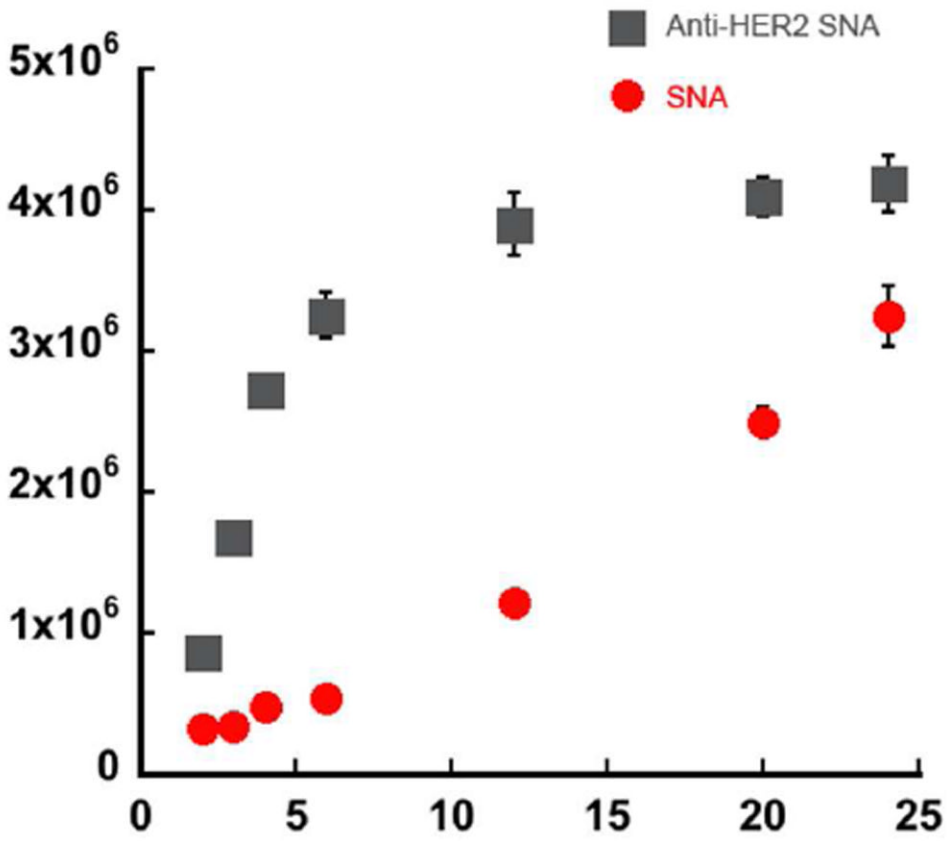

Figure 4.

Cell uptake of 5 nM targeted *vs.* non-targeted SNAs in SKOV-3 cells as a function of time. Targeted entry is more rapid at early time points (0-6 h), but becomes much slower at later time points. The difference in total particle uptake largely diminishes after 24 h.

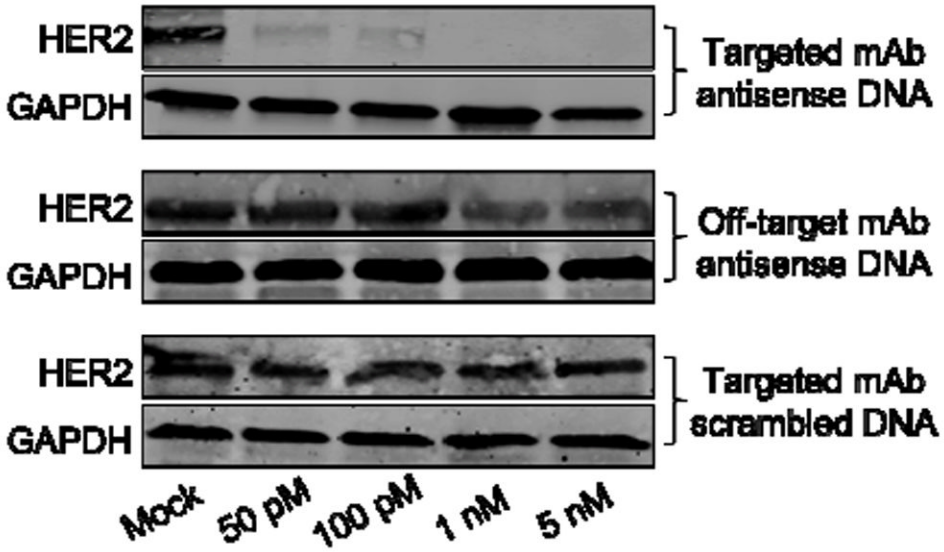

Figure 5.
Western blotting of HER2 expression in SKOV-3 cells after treatment with anti-HER2 SNAs and control samples. GAPDH is used as an internal reference.